RESEARCH ADVANCE

Figures and figure supplements

Emx2 regulates hair cell rearrangement but not positional identity within neuromasts

Sho Ohta *et al*

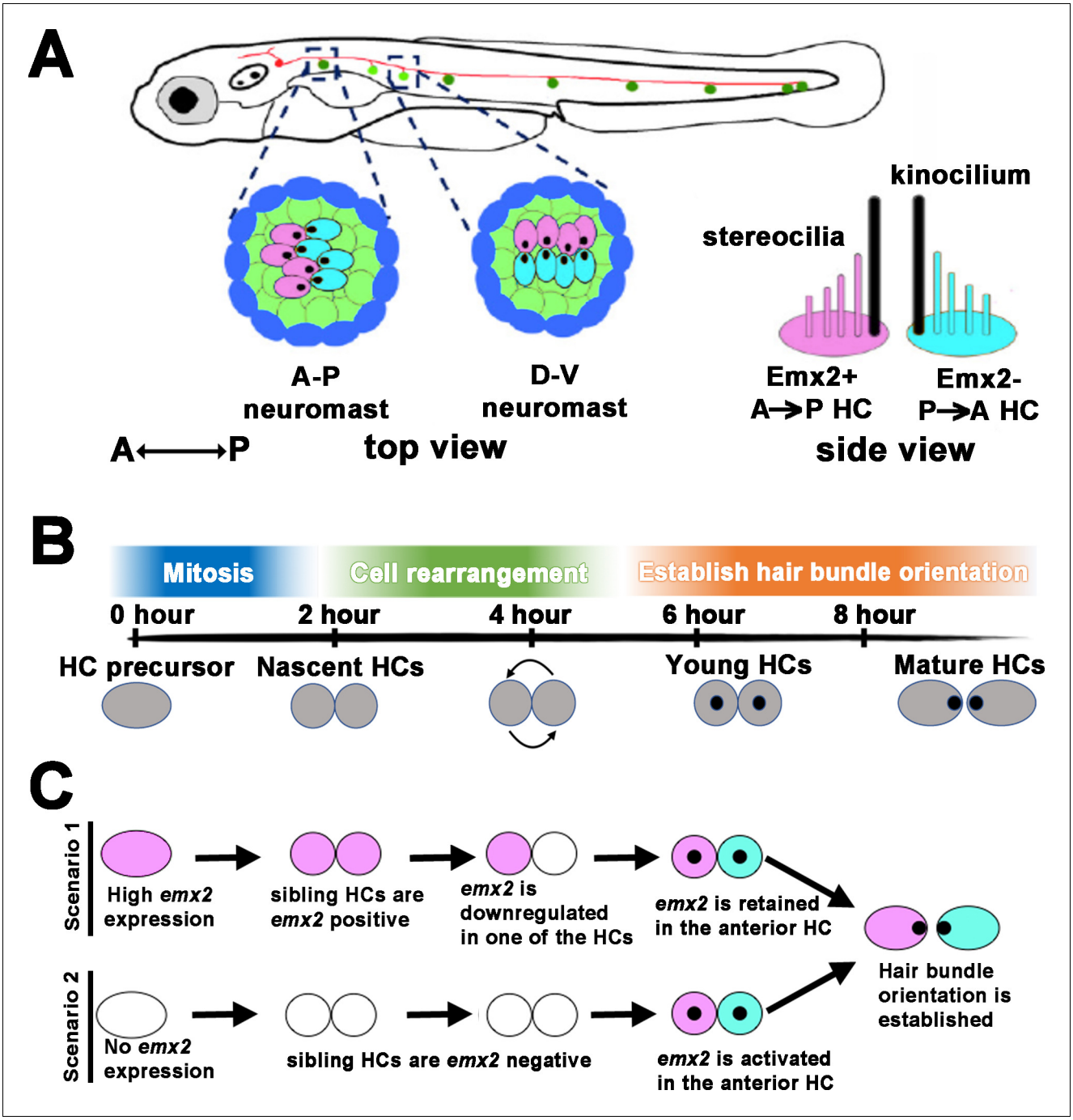

Figure 1. Schematic of bidirectional hair cell (HC) establishment in the zebrafish neuromast. (**A**) The lateral line system in zebrafish showing the top view of an anterior-posterior (A-P) and dorsal-ventral (D-V) neuromast, based on their hair bundle orientation. Side view of two hair bundles, each comprises a kinocilium (black) and a stereociliary staircase (pink or blue), arranged in opposite orientation atop of an Emx2-positive (pink) and Emx2-negative (blue) HC. (**B**) An approximate developmental time-line of HC formation in zebrafish neuromast. A HC precursor (gray) divides to form two daughter HCs, which roll to exchange positions with each other 50% of the time before differentiating into mature HCs with opposite hair bundle orientation. The entire process takes approximately 8 hr from detectable Gfp signal driven by the *myosin6b* promoter to HCs with polarized hair bundles based on our live-imaging analyses. (**C**) Emx2, which is important for establishing the bidirectional HC pattern, can be expressed early in the HC precursors, which could affect the HC rearrangement (scenario 1) or later during hair bundle establishment after HCs are formed (scenario 2). A combination of both scenarios is also possible (not shown). Black dots represent the position of the kinocilium.

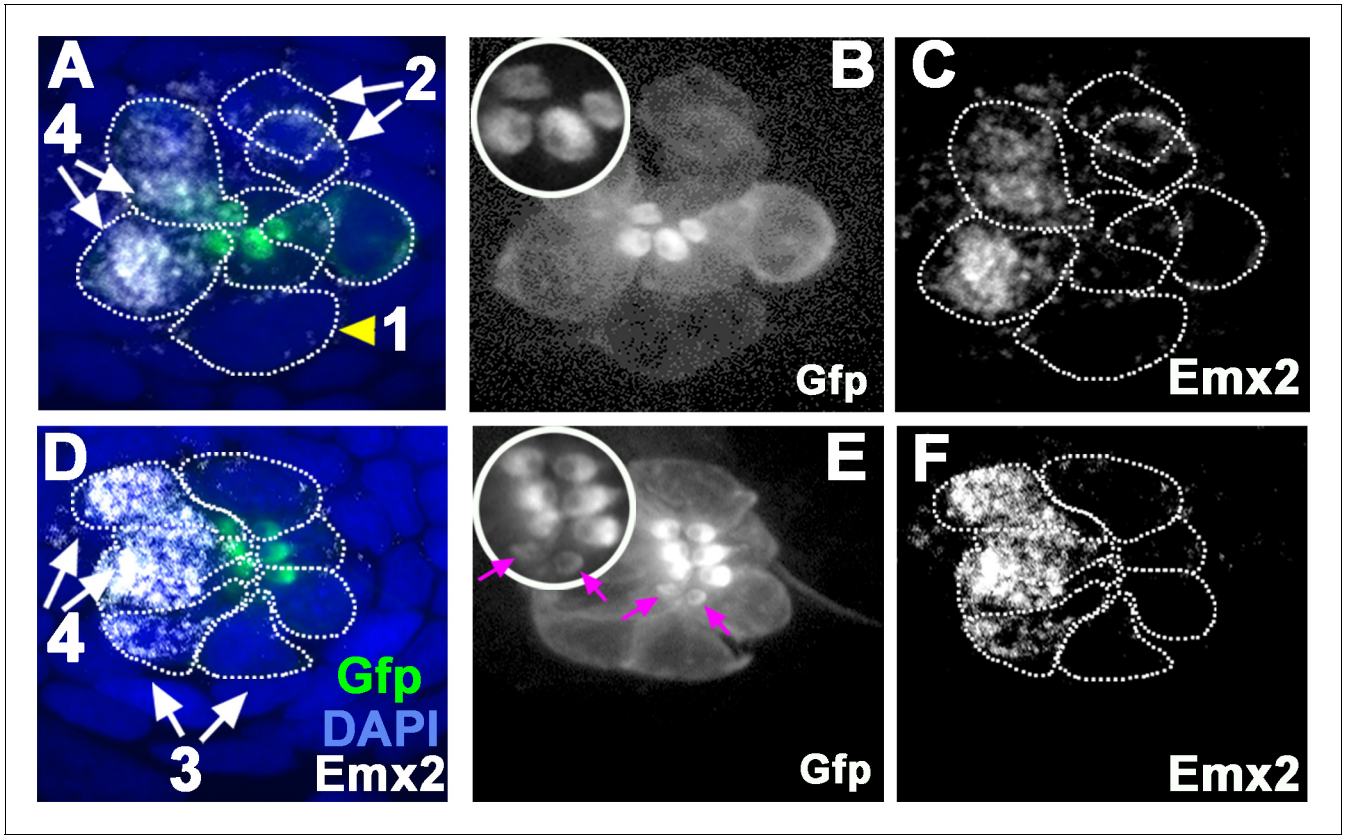

Figure 2. Emx2 immunostaining in wild-type (WT) (*myo6b:actb1-Gfp*) neuromasts. (**A and D**) Merged image of DAPI, (**B and E**) β-actin-GFP, and (**C and F**) anti-Emx2 staining of neuromasts. Emx2 immunoreactivity is not detected in dividing hair cell (HC) precursor (#1, arrowhead) or daughter HCs during Rock and Roll (#2). However, it is detectable in immature daughter HCs after Rock and Roll, in which the oriented hair bundle is not yet evident (#3, **E**, magenta arrows), as well as in mature HCs (#4). Both immature (#3) and mature HCs (#4, A→P) that are located in the anterior side of the neuromast are Emx2-positive. Insets in **B** and **E** are higher magnifications showing the hair bundle orientation pattern at the apex of HCs.

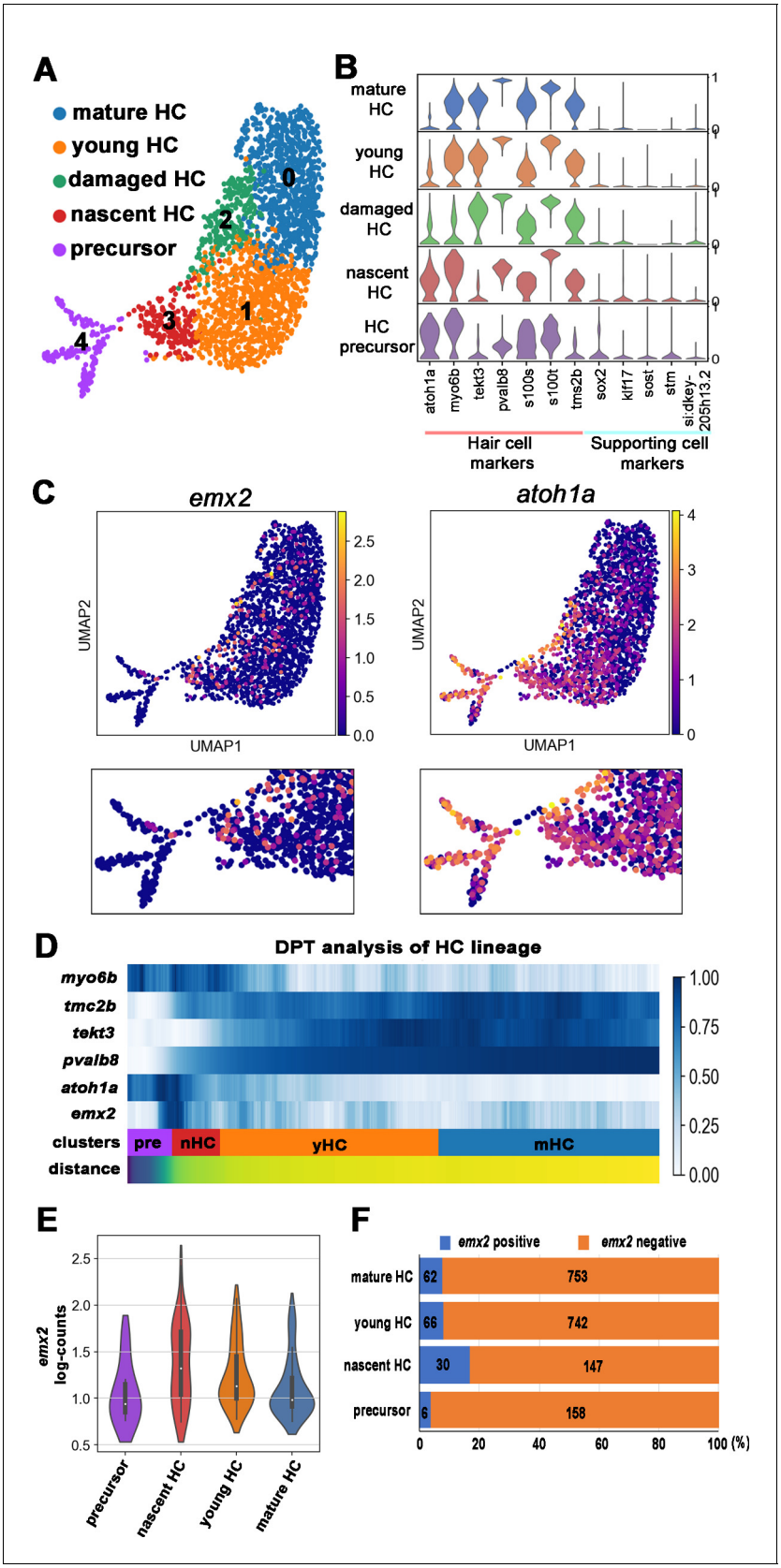

Figure 3. scRNA-seq analysis of the hair cell (HC) lineage in neuromasts. (**A**) Uniform manifold approximation and projection (UMAP) plot colored by Louvain clustering annotated with cell types in the HC lineage. (**B**) Violin plots of selected HC (red bar) and supporting cell (blue bar) marker genes in

Figure 3 continued on next page

Figure 3 continued

each cluster. (**C**) Distribution of cells expressing *emx2* and *atoh1a* on UMAP. Clusters of precursors (#4) and nascent HCs (#3) are enlarged in bottom panels. (**D**) Heat map representation of selected gene expression dynamics in pseudotime. (**E**) A violin plot showing significantly higher read counts of *emx2* in the nascent HC cluster than other clusters (p=0.0069, two tail Student's t-test, source data 1). (**F**) A bar graph showing a significantly higher number of *emx2*-positive cells in the nascent HC cluster than others (X^2 = 22.44, df = 3, p<0.0001, source data 2). A post-hoc 2 × 2 chi-squared test was also performed for multiple comparisons: precursor HC cluster vs nascent HC cluster, X^2 (df = 1)=15.92, p<0.0001; nascent HC cluster vs young HC cluster, X^2 (df = 1)=12.73, p=0.0004; nascent HC cluster vs mature HC, X^2 (df = 1)=15.08, p<0.0001. The following figure supplements are available for ***Figure 3—figure supplement 1***. Identification and annotation of cell types from Louvain clustering.

Figure 3—figure supplement 1. Identification and annotation of cell types from Louvain clustering. (**A**) Uniform manifold approximation and projection (UMAP) plot colored by Louvain clustering showing six clusters that included rpl10-HA (RiboTag) positive and negative cells. (**B**) Violin plots

Figure 3—figure supplement 1 continued on next page

Figure 3—figure supplement 1 continued

of selected marker genes of hair cell (HC) and SC. High levels of transgene tg_rpl10_3X_HA_short transcripts were concentrated in cluster #0, 1, 3, and 4 indicating they are cells within the HC lineage. Relative lower levels of rpl10-HA transcripts were found in cluster #2 of unknown identity, and #5, which expresses a high level of a SC marker, si:dkey-205h13.2. (**C**) Distribution of selected marker genes in UMAP. tg_rpl10_3X_HA_short is distributed in all the clusters except cluster #2. Supporting cell markers, si:dkey-205h13.2 and klf17 positive cells are concentrated in cluster #5. Thus, clusters #2 and #5 were excluded from the reclustering. (**D**) UMAP plot of reclustering of #0, 1, 3, and 4 shown in (**A**). (**E**) Heatmap showing the top 30 genes expressed in each cluster after the reclustering. (**F**) Violin plot showing distribution of n-counts, n-genes, mitochondrial fraction, and percentage of ribosomal genes of each cluster. The lower count depth, lower transcripts, and higher fraction of mitochondrial genes in cluster #2 indicate that they are damaged HCs. High percentages of ribosomal genes in clusters #3 and #4 are features of HC precursors and nascent HCs (***Lush et al., 2019***).

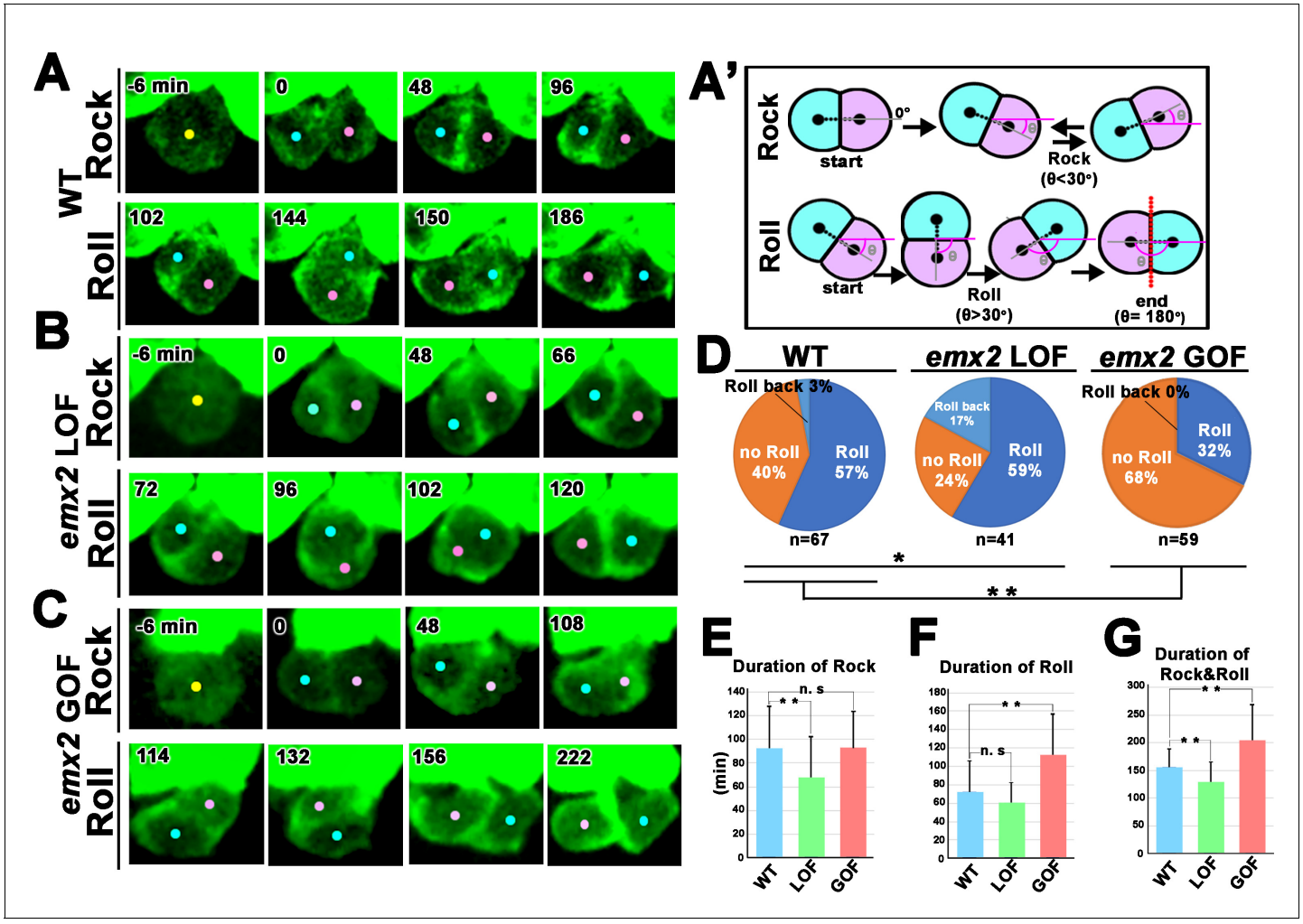

Figure 4. Quantification of frequency and duration of Rock and Roll among hair cells (HCs) in wild-type (WT) and *emx2* mutants. (**A**) In WT, a HC precursor (yellow dot) divides to form two daughter HCs (pink and blue dots), which first rock (Rock phase) and then frequently roll to exchange positions with each other (Roll phase). (**A'**) Definition of the Rock and Roll phase (see Materials and methods). (**B and C**) Compared to WT, *emx2* loss of function (LOF) (**B**) and gain of function (GOF) (**C**) HC pairs took a shorter time in Rock and Roll and a longer time in the Roll phase, respectively. (**D**) Frequencies of Roll, No Roll, and Roll back of nascent HC pairs in WT (n = 67 from seven larvae), *Emx2* LOF (n = 41 from six larvae), and GOF (n = 59 from seven larvae). Significance was assessed by using chi-squared test with 3 × 3 contingency table (X^2 (df = 4)=30.00, p<0.0001, source data 1). A post-hoc 2 × 3 chi-squared test was performed for multiple comparisons. WT vs. LOF; (X^2 (df = 2)=7.95, p=0.018), WT vs. GOF; (X^2 (df = 2)=10.39, p=0.0055). Post-hoc chi-squared tests were performed for pairwise comparisons with FDR correction. (**E–G**) Duration of Rock (**E**), Roll (**F**), and Rock and Roll (**G**) of sibling HCs that underwent Rock and Roll in WT (n = 42), *emx2* LOF (n = 35), and GOF (n = 19) larvae. Significance was assessed by using MANOVA (Rock, F(df1 = 2, df2 = 93)=5.349, p=0.0063, Wilks' λ = 0.897; Roll, F(df1 = 2, df2 = 93)=15.638, p<0.0001, Wilks' λ = 0.748; Rock and Roll, F (df1 = 2, df2 = 93)=20.10, p<0.0001, Wilks' λ = 0.698), with post-hoc Tukey's test for pairwise comparisons. *p<0.05, **p<0.01, n.s., not significant.

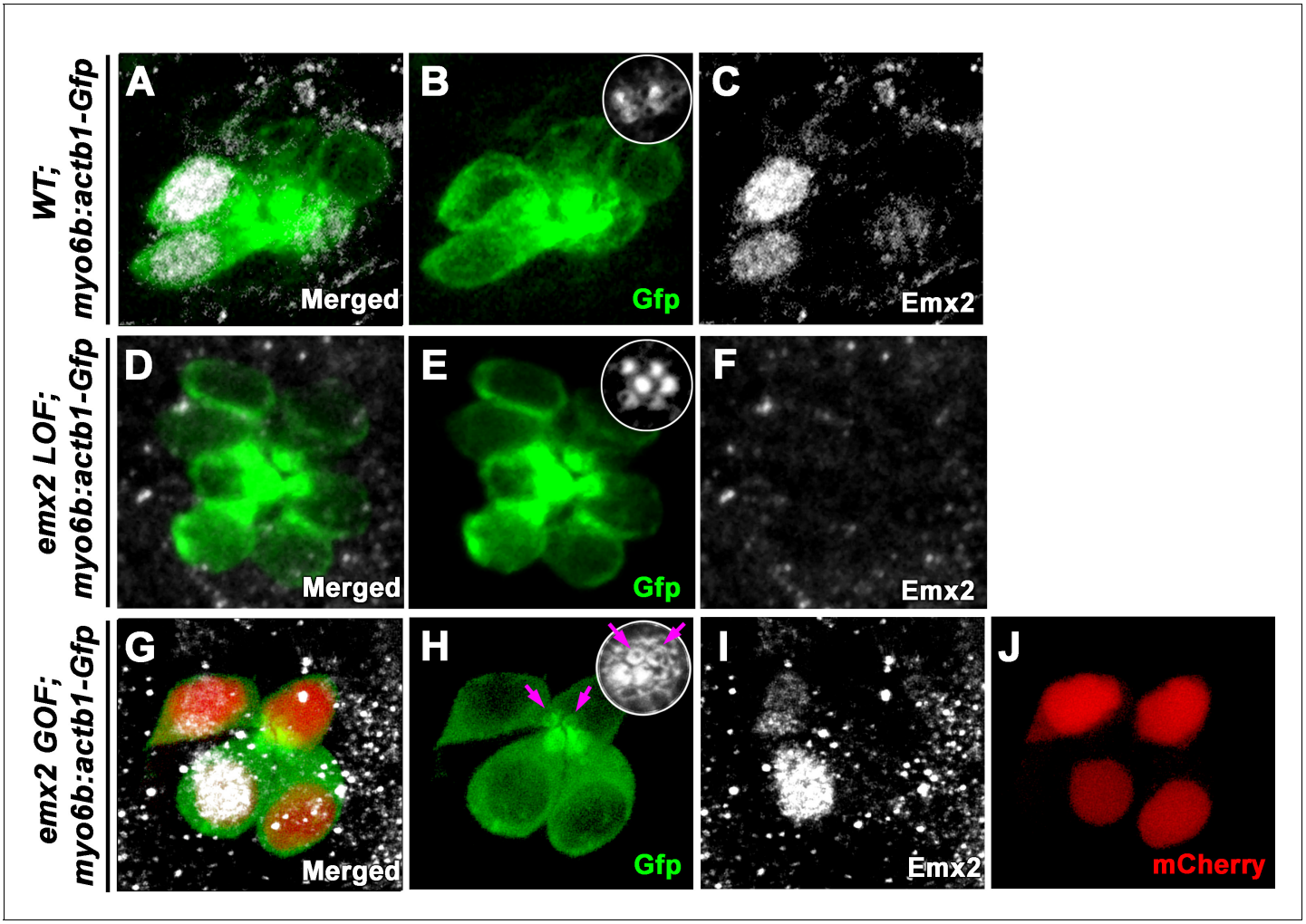

Figure 4—figure supplement 1. Localization of Emx2 expression in wild-type (WT), loss of function (LOF), and gain of function (GOF) neuromasts at 2.0 dpf. (**A–C**) Only hair cells (HCs) (**B**, Gfp) in the anterior neuromast of WT are positive for anti-Emx2 staining (**C**). Inset in B shows the bidirectional hair bundle orientation pattern. (**D–F**) No HCs (**E**) are positive for anti-Emx2 staining (**F**) in *emx2* LOF neuromast and all hair bundles are oriented in P→A direction (**E**). (**G–J**) An *emx2* GOF neuromast. (**G**) Merged image of Gfp (**H**), anti-Emx2 (**I**), and mCherry (**J**) expression. Anti-Emx2 staining only detected endogenous Emx2 in the anterior HCs (**I**), whereas exogenous Emx2 expression as indicated by mCherry expression is present in all HCs (**J**). All hair bundles are oriented in A→P direction and two immature HCs show the kinocilium located in the center (magenta arrows).

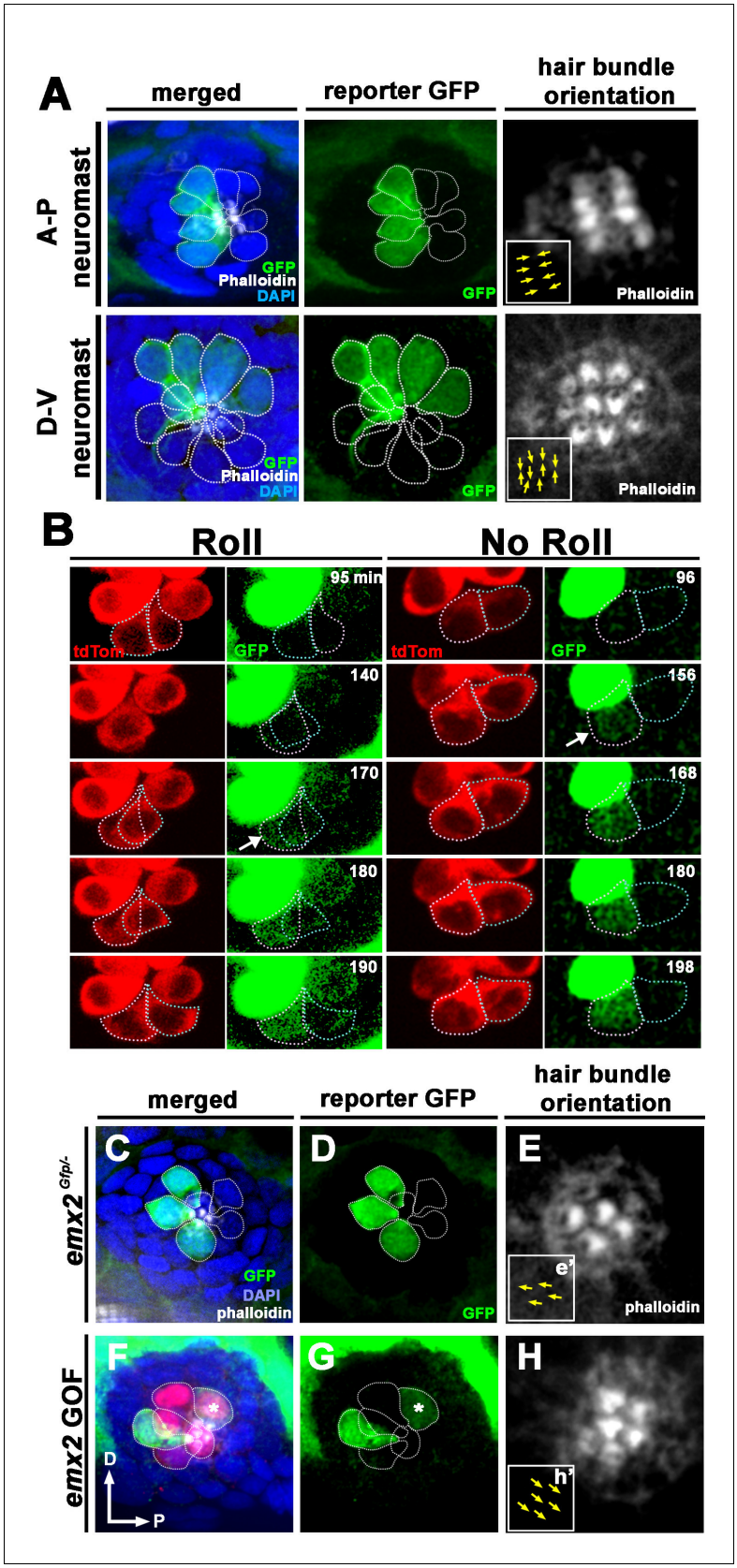

Figure 5. Spatiotemporal reporter activity of *emx2* in wild-type (WT) and *emx2* mutants. (**A**) In an *emx2:Gfp* zebrafish, Gfp-positive hair cells (HCs) are located in the anterior region of an A-P neuromast (top) and in the

Figure 5 continued on next page

Figure 5 continued

dorsal region of a D-V (bottom) neuromast. Phalloidin staining shows the hair bundle orientation (yellow arrows). (**B**) Time-lapse imaging of nascent HC pairs undergoing Roll or No Roll movement in *emx2:Gfp; myo6b:dtTomato* neuromasts. Left panel (Roll): A tdTomato-positive, nascent HC pair undergoing roll movement shows detectable Gfp expression in the posterior HC as it rolls into the anterior position (white arrow, 170 min into the Rock and Roll process). Right panel (No Roll): A HC pair that did not roll and Gfp appears in the anterior HC by 156 min into the Rock phase (white arrow). (**C–E**) The distribution of Gfp-positive HCs in an *emx2*$^{gfp/-}$ (loss of function [LOF]) neuromast, showing a merged image (**C**) of DAPI, GFP (**D**) and phalloidin staining (**E**). Outline of HCs are dotted. Gfp-positive HCs are located in the anterior region but hair bundles are pointing in P→A direction (yellow arrows in e'). (**F–H**) The distribution of Gfp-positive HCs in an *emx2* gain of function (GOF);*emx2*$^{Gfp/+}$ neuromast, showing a merged image (**F**) of DAPI, GFP (**G**), mCherry, and phalloidin staining (**H**). Among the total six pairs of GOF HCs analyzed, only two are Gfp-positive (**G**), one anterior- and one posterior (asterisk)-located. All hair bundles are in A→P direction (yellow arrows in h').

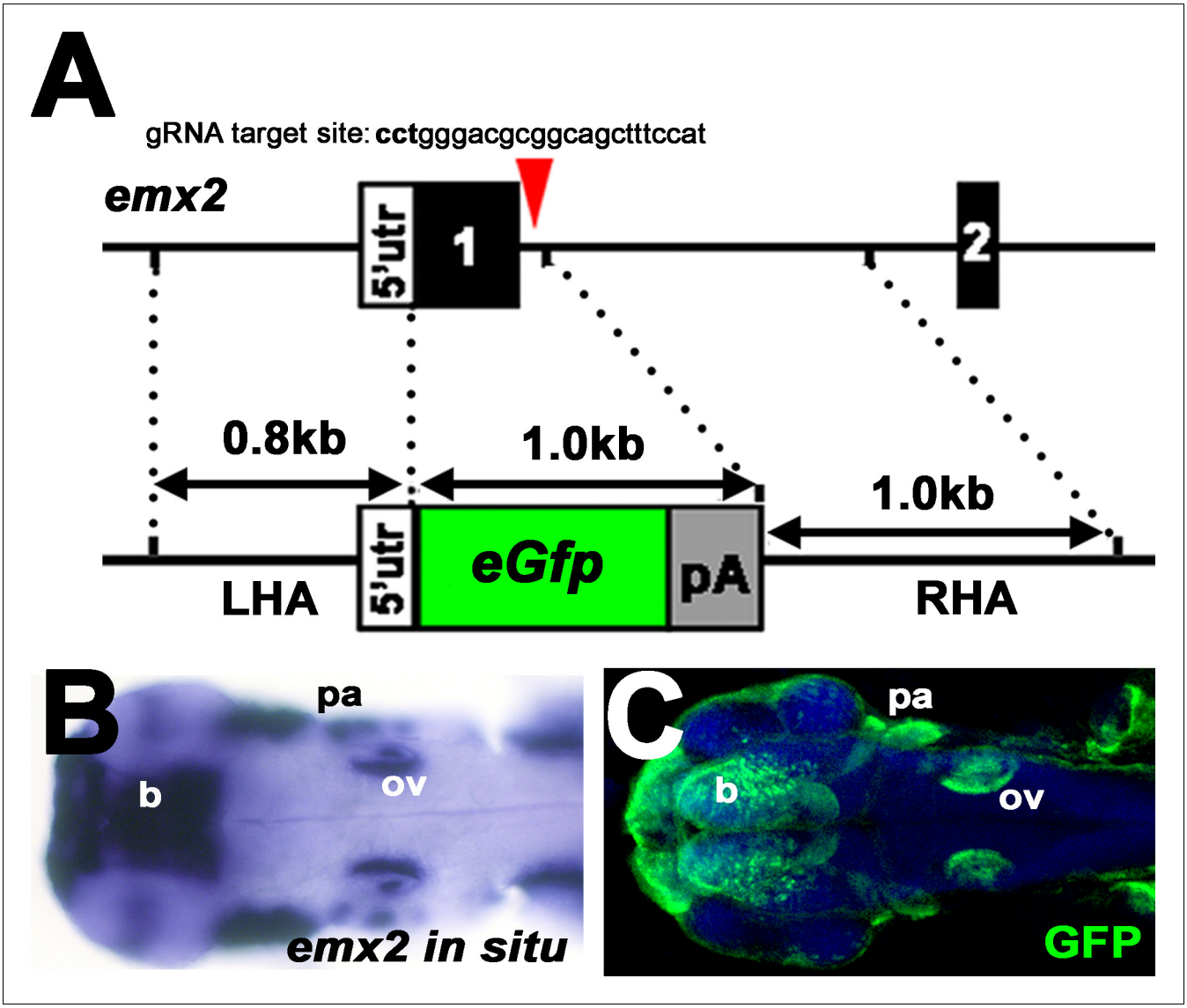

Figure 5—figure supplement 1. Generation of the *emx2:Gfp* transgenic line. (**A**) Schematic of the *emx2* genomic structure and its replacement with donor DNA using CRISPR. Red arrowhead indicates the target position for the guide RNA. The reporter *eGfp* and a polyA sequence in the targeting vector are flanked by left and right homologous arm (LHA and RHA) of the *emx2* allele as indicated with dotted line. The targeting position for the guide RNA is not included in either the LHA or RHA. (**B**) Hybridization signals of *emx2* transcripts in the brain (**b**), otic vesicles (ov), and pharyngeal arches (pa). (**C**) Gfp-positive regions in *emx2:Gfp* reporter larvae are similar to *emx2* positive regions indicated by in situ hybridization.

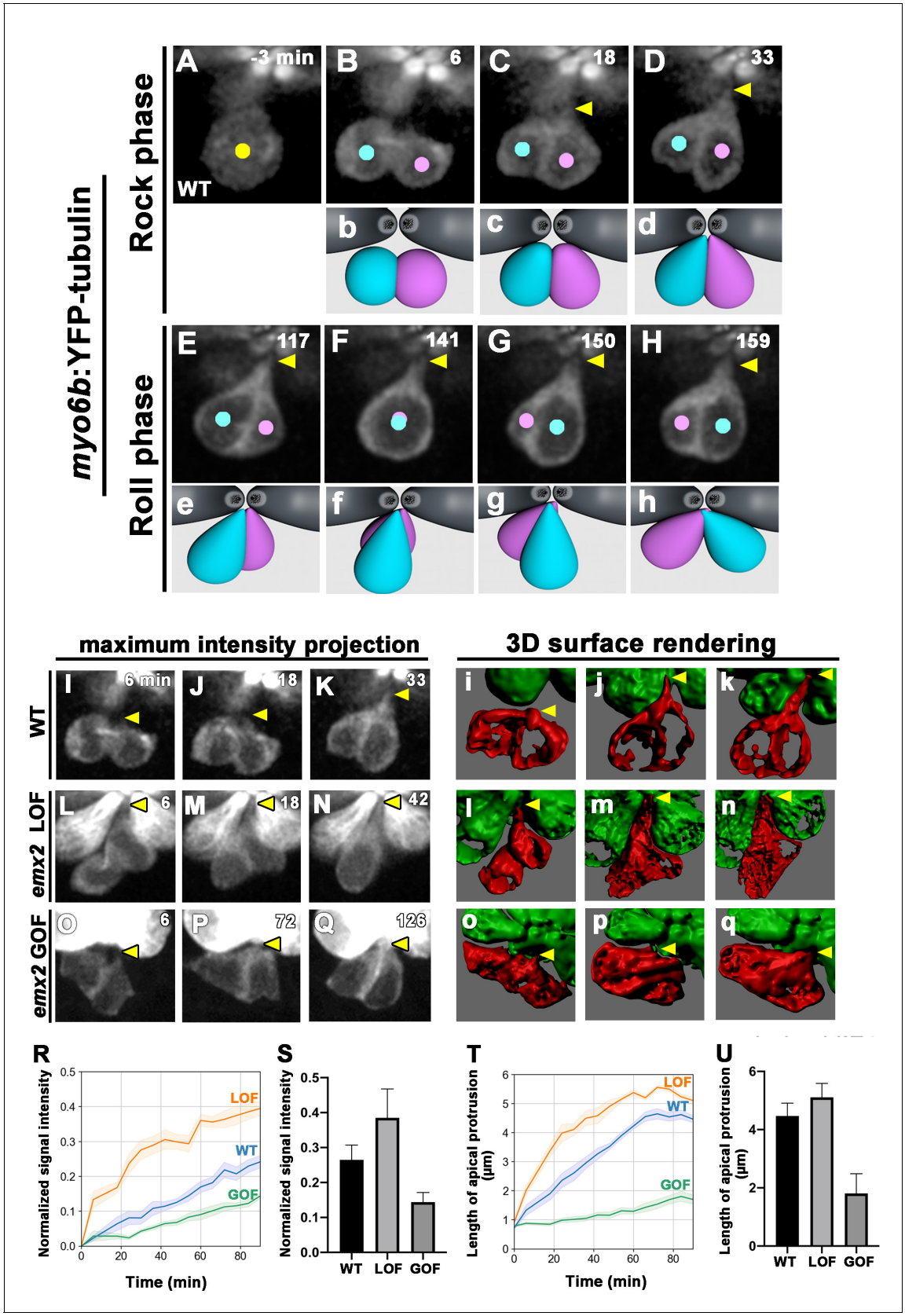

Figure 6. Emx2 affects apical protrusion formation in nascent hair cells (HCs). (**A–H**) Time-lapse images of *myo6b:YFP-tubulin* (wild-type [WT]) transgenic line showing nascent HCs undergoing Rock and Roll. After precursor cell divides (**A**), sibling HCs form an apical protrusion within 30 min of

Figure 6 continued on next page

Figure 6 continued

the Rock phase (**B–D**, yellow arrowhead, n = 6). When they exchange positions at the Roll phase, they appear to be pivoted at the apex (**E–H**, yellow arrowheads). Animation of images is shown in respective panels (Rock phase: **b–d**, Roll phase: **e–h**). (**I–Q**) Maximum intensity projection images generated by selected slices along z-axis in WT (**I–K**, same sample of **A–H**, n = 3), *emx2* loss of function [LOF] (**L–N**, n = 3) and *emx2* gain of function (GOF) (**O–Q**, n = 3). (**i–q**) Three-dimensional surface rendering of selected time points of live-imaging of HC pairs (red) in WT (**i–k**, n = 3), *emx2* LOF (**l–n**, n = 3), and *emx2* GOF (**o–q**, n = 3) neuromasts. Mature HCs are labeled in green. (**R**) Increases of YFP-tubulin signal intensity at the apical region of nascent HCs of WT (n = 5), *emx2* LOF (n = 5), and *emx2* GOF (n = 6) during the Rock phase (90 min). The shaded area represents the standard error of the mean (SEM). (**S**) YFP-tubulin signal intensities of the apical protrusion at the end of Rock phase were significantly different among WT (n = 5), *emx2* LOF (n = 5), and *emx2* GOF HCs (n = 6, one-way ANOVA, F = 26.97, p<0.0001); post-hoc Dunnett's multiple comparisons test for WT vs. LOF, p=0.0073, WT vs. GOF, p=0.0052. (**T**) Increases over time in the length of apical protrusion in WT (n = 5), *emx2* LOF (n = 5), and *emx2* GOF (n = 5) during the Rock phase (90 min). The shaded area represents the SEM. (**U**) The length of apical protrusion at the end of the Rock phase in WT (n = 5), *emx2* LOF (n = 5), and *emx2* GOF (n = 5) were compared. Significance was assessed by using one-way ANOVA, F = 52.15, p<0.0001. Post-hoc Dunnett's multiple comparisons test for WT vs. LOF is not significant (p=0.148) but significant for WT vs. GOF (p<0.0001). The following figure supplement, source data, videos are available for ***Figure 6—figure supplement 1***. Measurements of signal intensity and length of the apical protrusion using Image J Fiji.

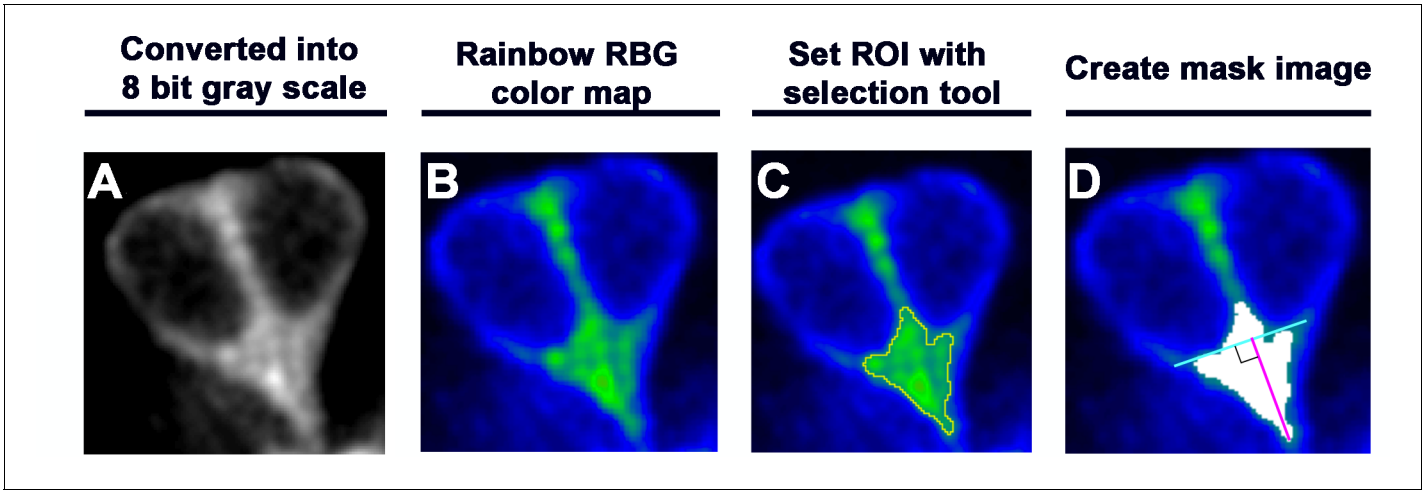

Figure 6—figure supplement 1. Measurements of signal intensity and length of the apical protrusion using ImageJ Fiji. (**A**) A selected maximum intensity projection image was converted into an 8-bit gray scale image. (**B**) The gray scale image in (**A**) was converted to Rainbow RBG color mode to visualize the bright green color of the accumulated YFP-tubulin within the apical protrusion. (**C**) Based on the signal intensity, the region of interest (ROI, yellow outline) was automatically defined by using the wand selection tool of ImageJ Fiji and the intensity measured. (**D**) The ROI was converted into a mask image (white area). A blue line was drawn across the top of the two hair cell (HC) nuclei, and a pink line joining the tip of the apical protrusion to the blue line at right angle indicates the length of the apical protrusion.

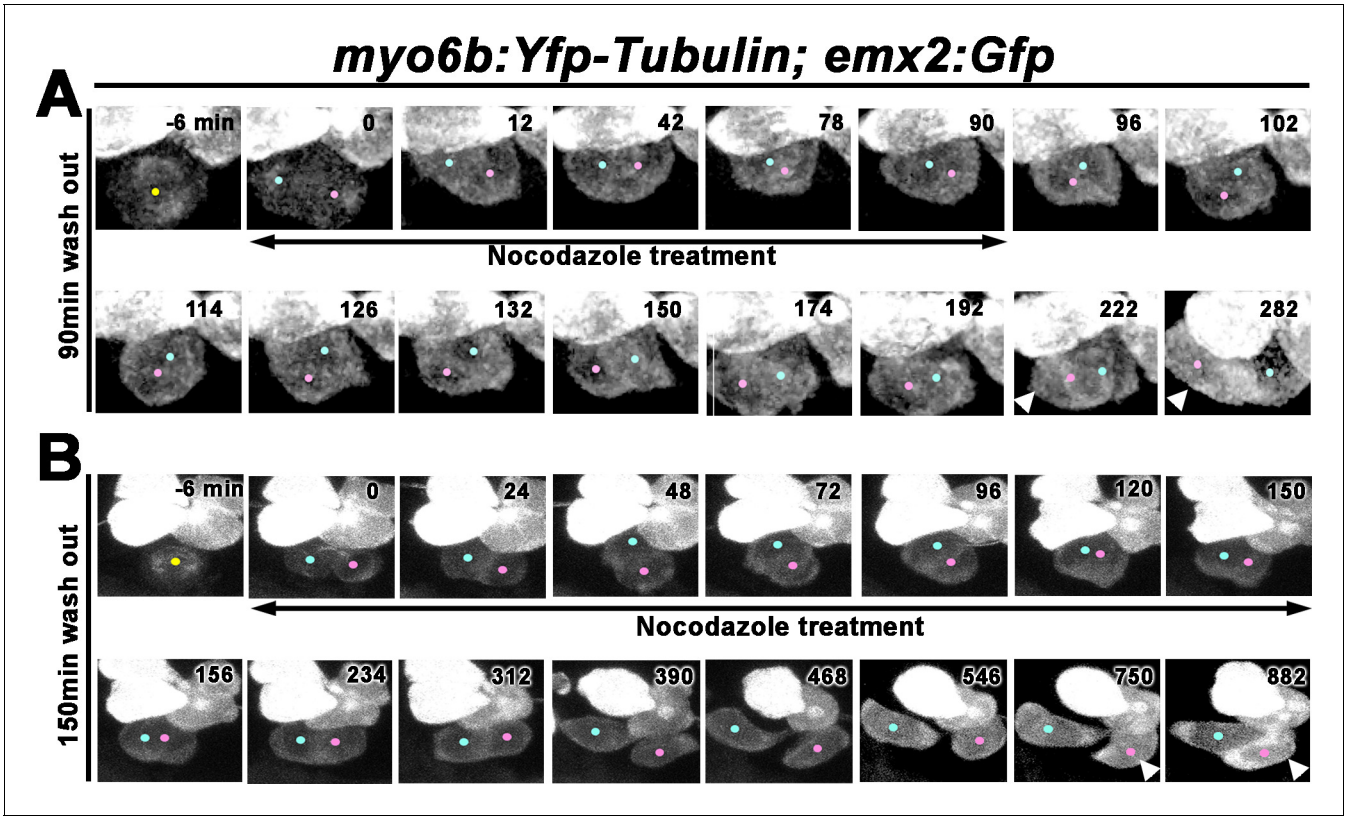

Figure 7. Nocodazole disrupts Rock and Roll and positional acquisition of hair cells (HCs). (**A**) Nascent sibling HCs in *myo6b:Yfp-tubulin; emx2:Gfp* larvae were treated with nocodazole for 90 min immediately after the HC precursor was observed to divide under live-imaging (0 min). After nocodazole removal, the nascent HC pair started to roll and they exchanged positions (96–174 min). The HC located at the anterior (pink dot) showed stronger Gfp signal due to the presence of *emx2:Gfp* and *Yfp-tubulin* alleles (222–282 min, arrowheads) than the *emx2:Gfp*-negative HC at the posterior (blue dot), which only expresses *Yfp-tubulin*. (**B**) Nascent HCs were treated with nocodazole for 150 min after HC precursor divided (0–150 min). After nocodazole removal, HCs failed to exchange their positions (156–312 min), which resulted in the mislocation of the *emx2:Gfp*-positive HC to the posterior (arrowheads, 618–882 min, pink dots).

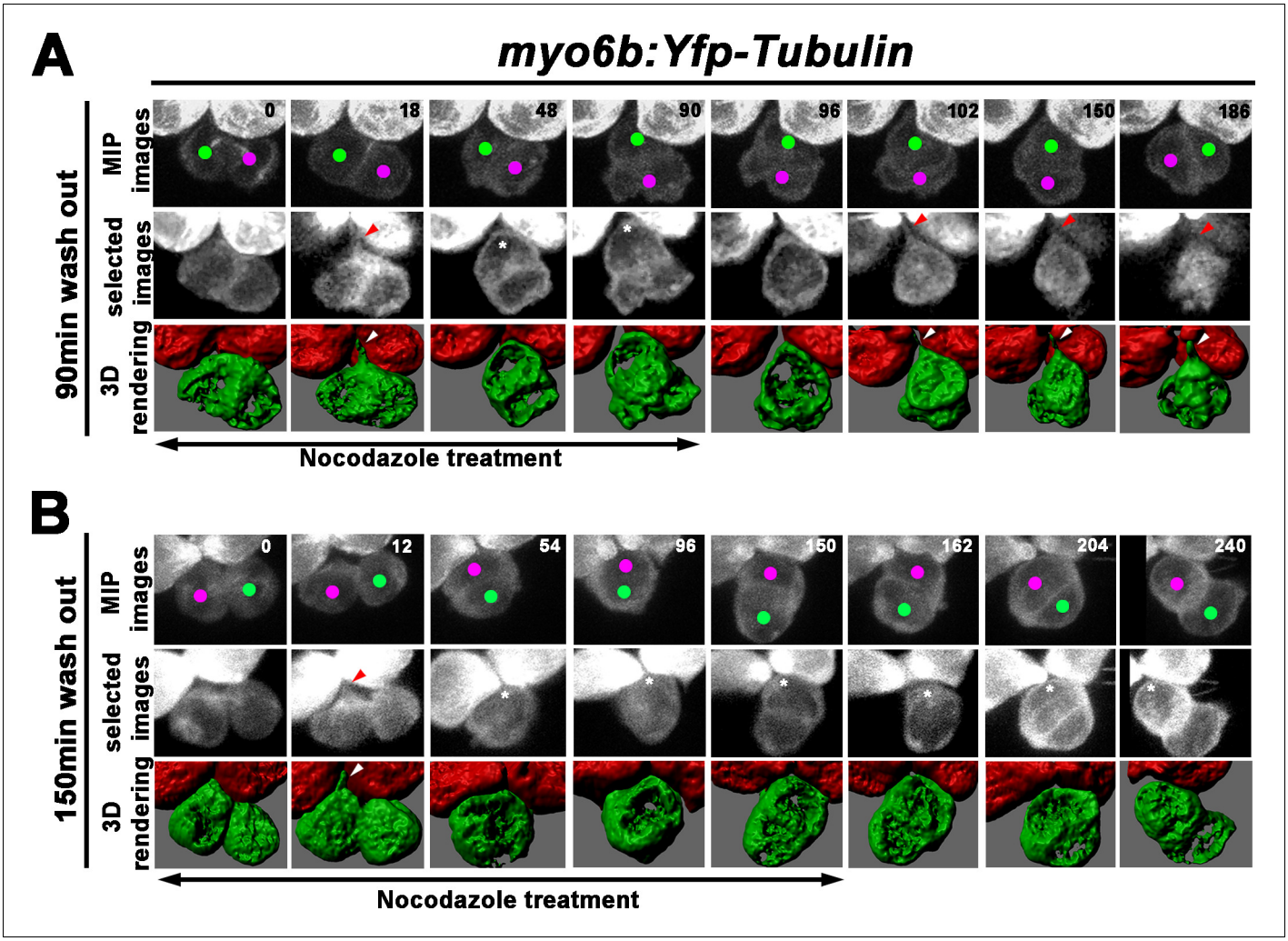

Figure 8. Formation of the apical protrusion is correlated with the Roll movement and hair cell (HC) positioning. (**A**) Maximum intensity projection and 3-D rendering of selected images of nascent sibling HCs in *myo6b:Yfp-tubulin* larvae (magenta and green dots) that was treated with nocodazole for 90 min immediately after the precursor divided. The apical protrusion that normally forms within 18 min was still evident initially (18 min; red and white arrowheads) but disappeared quickly between 30 and 36 min (asterisks, 48 min). After nocodazole removal, the apical protrusion reappeared after 12 min (102 min, red and white arrowheads) and the two nascent HCs rolled to their respective positions after 84 min (186 min). (**B**) A nascent HC pair (red and green dots) that was treated with nocodazole for 150 min immediately after the precursor divided. Similar to 90 min treatments, the apical protrusion was evident between 12 and 18 min (12 min, red and white arrowheads) after HC precursor divided (0 min) but disappeared shortly within 30–36 min (54 min, asterisk). However, after nocodazole removal at 150 min, sibling HCs did not form an apical protrusion and exchange positions (162–240 min, asterisks).

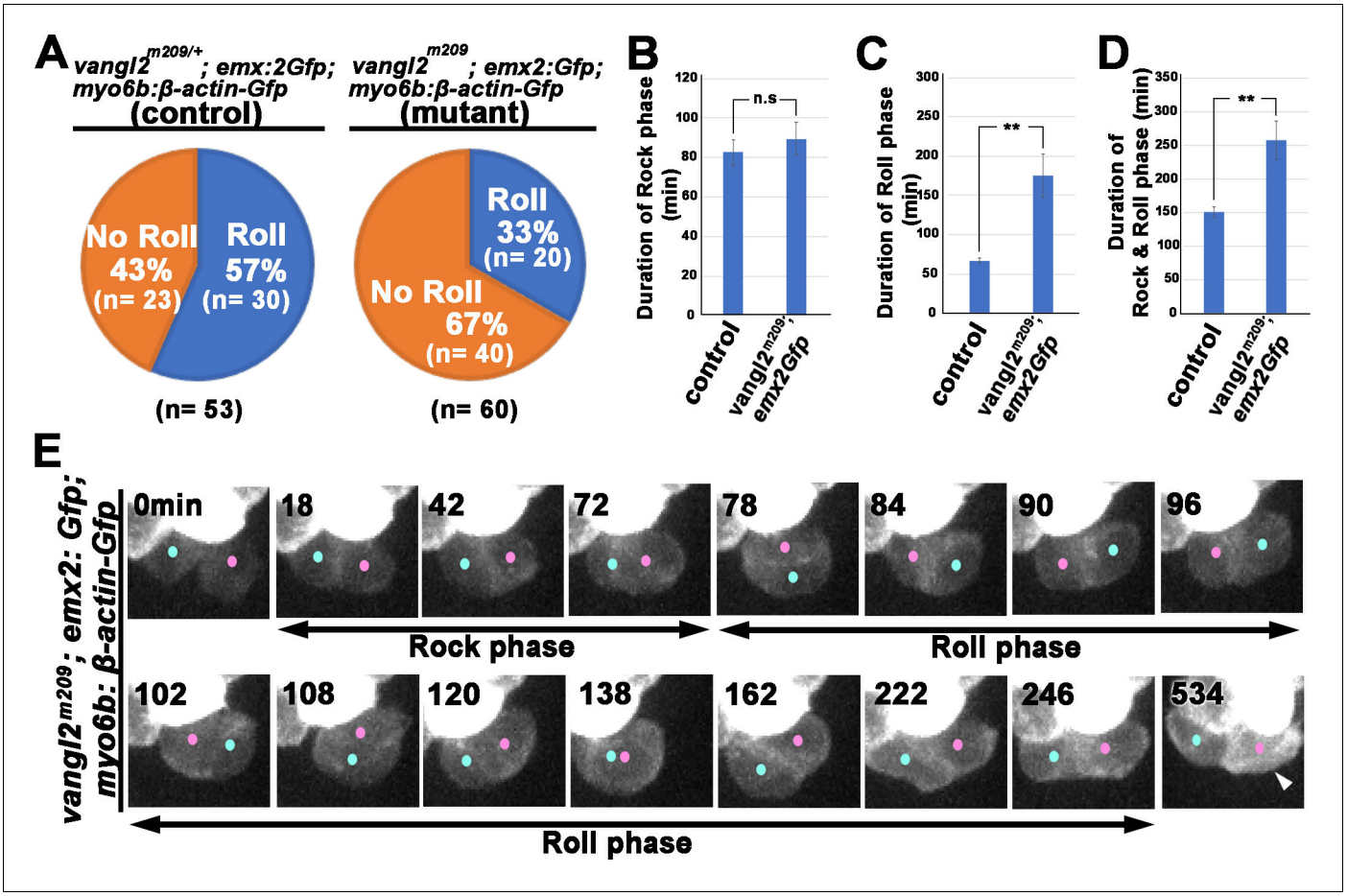

Figure 9. Rock and Roll is affected in the core planar cell polarity (cPCP) mutant, *trilobite*. (**A**) Frequencies of Roll and No Roll of nascent hair cell (HC) pairs in control (*vangl2*$^{m209/+}$; *emx2*$^{gfp/+}$) and mutant (*vangl2*$^{m209/m209}$; emx2$^{gfp/+}$) larvae. Significance was assessed by using chi-squared test with a 2 × 2 contingency table (X^2[(df = 1)]=6.1774, p<0.013, source data 1). (**B–D**) Duration of Rock (**B**), Roll (**C**), and Rock and Roll (**D**) of sibling HCs that underwent Rock and Roll in control (n = 28 from seven larvae) and *vangl2*$^{m209/m209}$; *emx2*$^{gfp/+}$ (n = 19 from seven larvae) larvae. Significance was assessed by using Student's t-test (*p<0.05, **p<0.001, source data 2). The error bars represent SEM. (**E**) Time-lapse images of a HC pair in *trilobite* (*vangl2*$^{m209/m209}$); *emx2*$^{gfp/+}$ mutant, which undergoes a prolong Roll phase from 78 to 246 min with several rolls (first roll: 78–96 min, second roll: 102–120 min, third partial roll: 138–162 min) and resulted in the *emx2:Gfp*-positive HC located to the posterior. The following figure supplement, source data, and video are available for ***Figure 9—figure supplement 1***. Formation of apical protrusion in nascent HCs of *trilobite*.

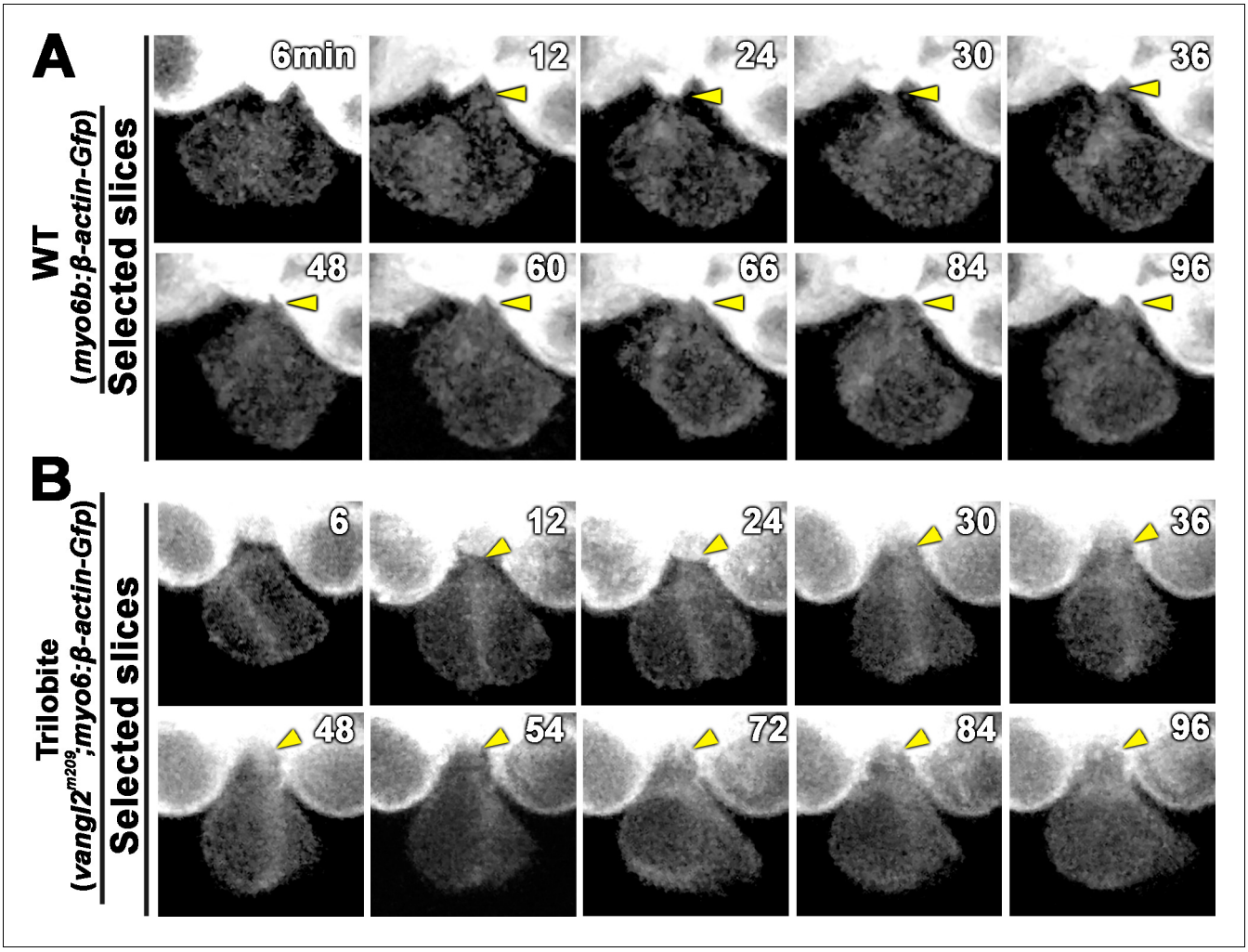

Figure 9—figure supplement 1. Formation of apical protrusion in nascent hair cells (HCs) of *trilobite*. Time-lapse images of a nascent HC pair during Rock phase in (**A**) wild-type (WT) (*myo6:β-actin-Gfp*) and (**B**) *trilobite* larvae. The apical protrusion (yellow arrowhead) was evident by 12 min after the HC precursor divided in both WT and mutant.

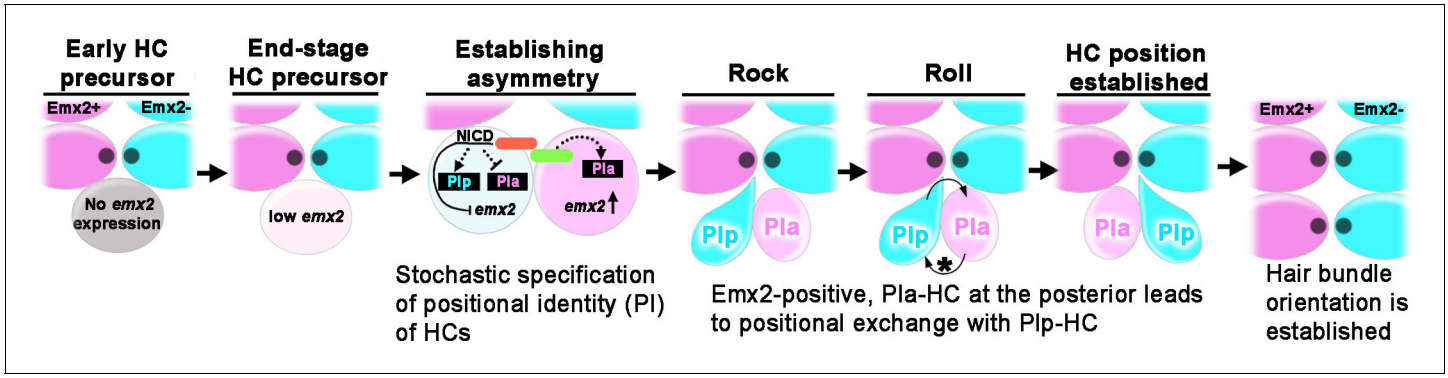

Figure 10. Model of positional acquisition of nascent hair cells (HCs) in the neuromast. Unlike scenarios 1 and 2 illustrated in ***Figure 1C***, our results show a model in which an end-stage HC precursor before division expresses low levels of *emx2* (light pink). After the precursor divided, Notch signaling mediated through the Notch ligand (green color) and Notch1a receptor (red color) generates asymmetry between the two sibling HCs. This asymmetry results in stochastic specification of anterior (Pla) and posterior (Plp) positional identity (PI) to sibling HCs, which includes regulation of *emx2* expression. Thus, an *emx2*-positive, Pla-HC formed at the posterior position undergoes positional exchange with its sibling Plp HC, whereaswhen an *emx2*-positive, Pla-HC formed in the anterior position, the two sibling HCs do not exchange positions. In addition to the delay in apical protrusion mediated by Emx2, the Rock and Roll is also regulated by the intercellular core planar cell polarity (cPCP) pathway (asterisk).